



Original Paper

A developed transient gas–liquid–solid flow model with hydrate phase transition for solid fluidization exploitation of marine natural gas hydrate reservoirs



Geng Zhang^a, Jun Li^{a,b,*}, Gong-Hui Liu^a, Hong-Wei Yang^a, Chao Wang^a,
Hong-Lin Huang^a

^a China University of Petroleum-Beijing, Beijing, 102249, China

^b China University of Petroleum-Beijing at Karamay, Karamay, 834000, Xinjiang, China

ARTICLE INFO

Article history:

Received 11 March 2022

Received in revised form

2 November 2022

Accepted 5 November 2022

Available online 11 November 2022

Edited by Yan-Hua Sun

Keywords:

Gas–liquid–solid multiphase flow

Solid fluidization

Hydrate dynamic decomposition

Convective heat transfer

ABSTRACT

The multiphase flow characteristic is one of the most concerning problems during solid fluidization exploitation of marine natural gas hydrate reservoirs. In this research, a new transient gas–liquid–solid multiphase flow model with hydrate phase transition was developed. Meanwhile, this model considered the coupling relationship among convective heat transfer, hydrate dynamic decomposition, and multiphase flow. The model can simulate the change of flow pattern from solid–liquid to gas–liquid–solid flow, and describe the distribution character of volume fraction of phase, wellbore temperature and pressure, and hydrate decomposition rate during transportation. The simulation results indicate that the hydrate decomposition region in the wellbore gradually expands, but the hydrate decomposition rate gradually decreases during the solid fluidization exploitation of hydrate. When mining time lasts for 4 h, and the bottom hole pressure decreases by about 0.4 MPa. Increasing NaCl concentration in seawater helps expand hydrate decomposition regions and improves the wellbore hydrate decomposition rate. When the NaCl mass fraction in seawater reaches 15%, it will raise the hydrate decomposition regions to the whole wellbore. In addition, the higher the wellhead backpressure, the lower the decomposition area and decomposition rate of hydrate in the wellbore. When wellhead backpressure reaches 2 MPa, the volume fraction of gas near the wellhead will reduce to about 12%. This work is expected to provide a theoretical basis for the development of marine hydrate reservoirs.

© 2022 The Authors. Publishing services by Elsevier B.V. on behalf of KeAi Communications Co. Ltd. This is an open access article under the CC BY-NC-ND license (<http://creativecommons.org/licenses/by-nc-nd/4.0/>).

1. Introduction

The natural gas hydrate (NGH) is commonly known as “combustible ice,” a new clean and nonpolluting energy. It has the particularity of wide distribution, high calorific value, high density, and so on (Bai et al., 2009; Boswell and Collett, 2011; Zhao et al., 2022). At present, the hydrate resources detected worldwide are mainly stored in polar sandstones and marine sandstones. This kind of hydrate resource with good closure can be developed conventionally. However, while mining, the metastable NGH stored within a few hundred meters on the seabed needs to adopt a new

exploitation method. This type of NGH has the particularities of shallow burial depth, no tight cover, loose mineral deposits, low cementation degree, and easy fragmentation. If the mining is carried out conventionally, it will directly cause many decompositions, gasification, and gas-free release of the weak cement hydrate, which is a waste of resources and causes environmental pollution and damage (Guo et al., 2016; Yang et al., 2019b; Sun et al., 2020).

For this challenging problem, Zhou et al. proposed a solid fluidization method to exploit the NGH resources in the seabed's external surface, as shown in Fig. 1 (Zhou et al., 2017; Zhao et al., 2017). This method's basic idea is that the natural gas hydrate-bearing sediments (NGHBS) are crushed into small particles and disposed of by the fluidization process through mechanical mining and secondary crushing. Then, the NGHBS are mixed with seawater. Finally, the NGHBS are transported to the offshore platform through pipelines for later treatment.

* Corresponding author. China University of Petroleum-Beijing, Beijing, 102249, China.

E-mail address: lijun446@vip.163.com (J. Li).

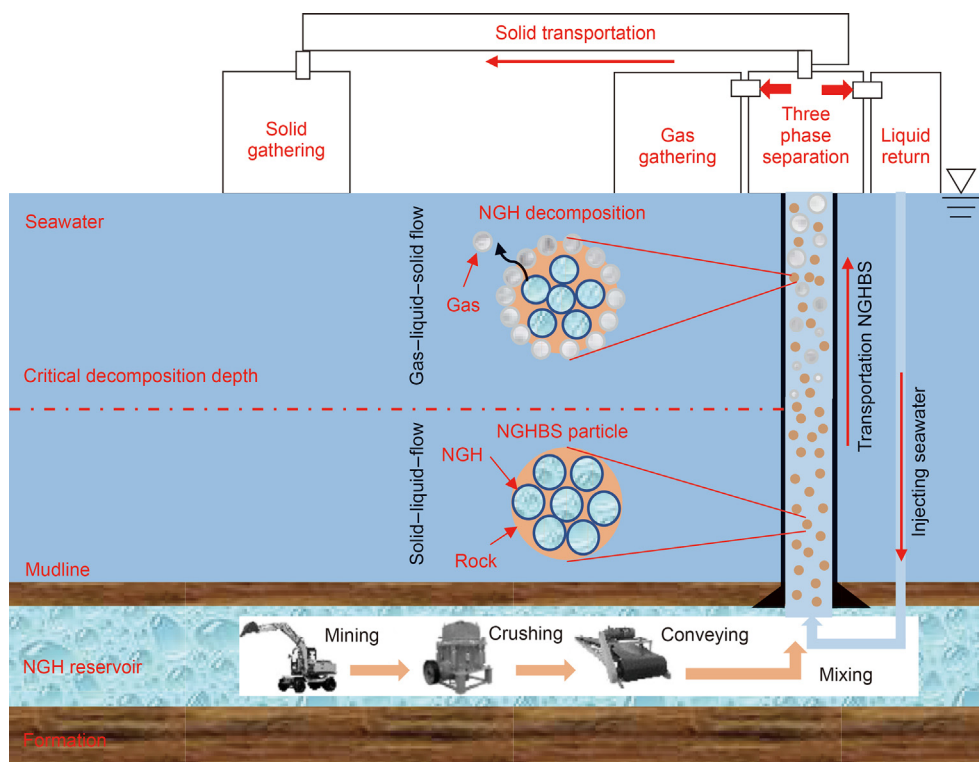


Fig. 1. Mechanisms of multiphase flow coupling hydrate dynamic decomposition during solid fluidization exploitation.

process. Gao et al. (2017a, b) developed a multiphase flow model coupled with temperature and pressure during hydrate formation drilling with riser. Wei et al. (2016) considered the interaction of stress, hydrate decomposition, and velocity in the drilling process of the NGH reservoir. They studied the hydrate decomposition law and multiphase flow rule under different operating parameters. However, the heat and mass transfer between phases caused by hydrate decomposition was not considered in the model, so the accuracy of obtained phase volume fraction and temperature is poor. Sun et al. (2018) analyzed the coupled hydrate phase transition and overflow process and developed a unified gas-liquid flow mechanism model. Unfortunately, the coupled relationship between the hydrate dynamic decomposition and the wellbore heat transfer was ignored. Liao et al. (2019) established a gas-liquid-solid flow model to simulate the drilling process of hydrate formation. However, the model assumed that hydrate start to decomposition from the bottom of the well. Li et al. (2019) established a gas-liquid-solid transient flow model, which considered multiphase flow and hydrate decomposition. Based on developed model, he used CFD software to simulate the multiphase flow characteristics during mechanical-thermal exploitation of NGH. However, the size of the established geometric model is small. The simulated wellbore length is only 1.5 m, which cannot describe the pressure changes along the wellbore in the actual hydrate mining process.

It can be seen that the above multiphase flow model considering hydrate phase transition mainly simulates the drilling process of hydrate formation and the gas kick process of deepwater drilling, but there are few multiphase flow models simulating the solid fluidization exploitation of NGH reservoirs. In addition, the existing models do not comprehensively consider the coupling relationship among multiphase flow, convective heat transfer, and hydrate decomposition. Therefore, it's necessary to research the hydrate

decomposition law and the multiphase flow rule during solid fluidization exploitation of NGH. This will provide some theoretical reference for the safe and efficient exploitation of Marine shallow gas hydrate.

2. Mathematical model

As shown in Fig. 2, there are multiple physical processes in the wellbore during the solid fluidization exploitation of the NGH, including multiphase flow, convective heat transfer between the surrounding medium and the fluid, interphase heat and mass transfer resulted from hydrate decomposition, and changes in the fluid properties and wellbore pressure. The coupling relationship between these physical processes can be summarized as follows:

- (1) The convective heat transfer between the fluid and the surrounding medium affects the fluid temperature, and then the hydrate decomposition rate, wellbore pressure, and multiphase flow characteristics.
- (2) The interphase heat and mass transfer caused by hydrate decomposition will affect the phase volume fraction and wellbore temperature, and then the wellbore pressure, convective heat transfer coefficient, and wellbore flow characteristics.
- (3) The multiphase flow of the decomposition gas, seawater, and hydrate particles in wellbore affects mixture velocity and wellbore pressure, and then hydrate decomposition rate.

Besides, the type of flow in the wellbore will change from solid-liquid flow to gas-liquid-solid flow when hydrate particles reach the critical depth of phase transient. To establish a gas-liquid-solid flow mechanism model coupled hydrate dynamic decomposition, wellbore temperature, and multiphase flow, the main assumptions

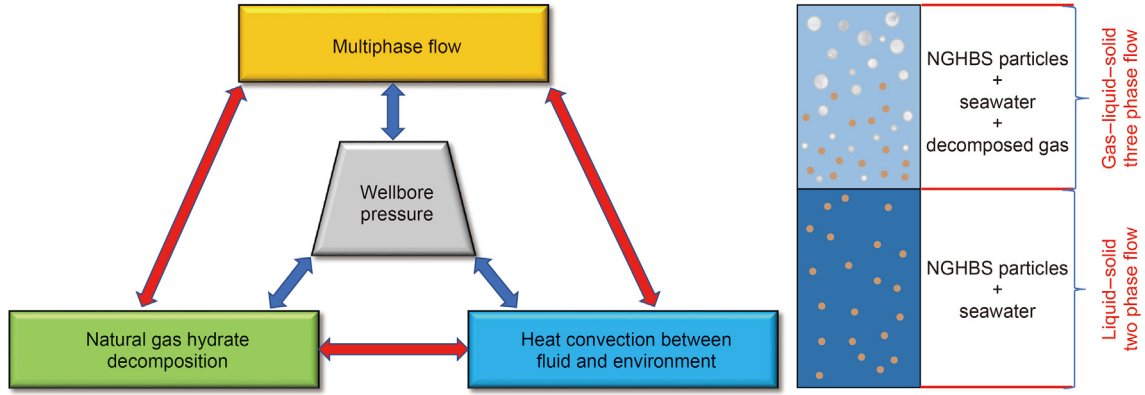


Fig. 2. The coupling relationship between hydrate decomposition, multiphase flow and heat transfer.

are as follows (Yang et al., 2019a; Li et al., 2019; Liao et al., 2019):

- (1) The flow in the wellbore is regarded as a one-dimensional flow.
- (2) Hydrate particles are regarded as spherical ideally, and will not collapse during dissociation.
- (3) Ignoring the effects of Joule-Thomson and adiabatic cooling on wellbore temperature field.
- (4) Assume that the thermal properties of seawater, casing, and rock do not change.
- (5) The hydrate particles are treated as a continuous phase.

2.1. Mass conservation equations

Considering the natural gas hydrate decomposition during solid fluidization exploitation of marine gas hydrate reservoirs, the mass conservation equations for decomposed gas, seawater and hydrate particle are expressed as (Wei et al., 2019; Li et al., 2019; Liao et al., 2019):

$$\frac{\partial(A\rho_g\alpha_g)}{\partial t} + \frac{\partial(A\rho_g\alpha_g v_g)}{\partial z} = A\alpha_s \dot{m}_g \quad (1)$$

$$\frac{\partial(A\rho_l\alpha_l)}{\partial t} + \frac{\partial(A\rho_l\alpha_l v_l)}{\partial z} = q_l + A\alpha_s \dot{m}_l \quad (2)$$

$$\frac{\partial(A\rho_s\alpha_s)}{\partial t} + \frac{\partial(A\rho_s\alpha_s v_s)}{\partial z} = q_s - A\alpha_s \dot{m}_h \quad (3)$$

To solve the complex multiphase flow problem, Zuber and Findlay (1965) built the drift flow model considering the phase slip effect. Compared with the homogeneous phase flow model and the separated phase flow model, the drift flow model is more consistent with the actual flow law and simpler to calculate. Based on the definition of drift flow, the actual velocity of the gas phase and the solid phase is described as:

$$v_g = C_g v_m + v_{gr} \quad (4)$$

$$v_s = C_s v_f - v_{sr} \quad (5)$$

Then gas distribution coefficient c_g and gas drift velocity v_{gr} have been widely researched in oil and natural gas fields. Shi et al. (2005) obtained widely accepted empirical formulas of gas distribution coefficient and gas drift velocity through a large number of experiments. The c_g and v_{gr} are presented as follows

$$c_g = \frac{A_e}{1 + (A_e - 1)\gamma^2} \quad (6)$$

$$v_{gr} = \frac{c_g v_c (1 - \alpha_g c_g) K(\alpha_g)}{1 - \alpha_g c_g \left[1 - (\rho_g/\rho_l)^{1/2}\right]} (\cos\theta)^{1/2} (1 + \sin\theta)^2 \quad (7)$$

Considering the small amount of NGH decomposition in the mining process, the wellbore flow pattern is mainly bubbly flow or dispersed bubbly flow, and here approximately regard as $v_f = v_m$. According to Lyoho's research, $c_s = 1$. He (2016) introduced the angle correction factor and obtained the empirical settling velocity model. The expression of settling velocity is:

$$v_{sr} = 0.223 \frac{e^{5.03\phi} \mu'_m}{\rho'_m d_s} \sin\theta \left[\sqrt{1 + 0.399g \frac{(\rho_s - \rho'_m)\rho'_m d_s^3}{e^{5.03\phi} \mu'^2_m}} - 1 \right] \quad (8)$$

2.2. Momentum conservation equations

According to the momentum theorem, the mixed momentum conservation equation of gas-liquid-solid is described as

$$\begin{aligned} & \frac{\partial}{\partial t} \sum_{m=g,l,s} (\rho_m \alpha_m v_m A) + \frac{\partial}{\partial z} \sum_{m=g,l,s} (\rho_m \alpha_m v_m^2 A) \\ & + \sum_{m=g,l,s} (\rho_m \alpha_m) A g \sin\theta + \frac{\partial(pA)}{\partial z} + \frac{\partial(p_f A)}{\partial z} + (q_s v_s + q_l v_l) \\ & + (\dot{m}_g v_g + \dot{m}_l v_l - \dot{m}_h v_s) \\ & = 0 \end{aligned} \quad (9)$$

2.3. Energy conservation equations

In the process of hydrate particle transportation, the temperature of the mixture depends on the following processes: (1) Heat is transferred along the axial direction with fluid motion; (2) Heat convection between the fluid and the wall; (3) Heat absorbed by the decomposition of hydrate. Therefore, the energy conservation equation of the mixture can be expressed as:

$$\frac{\partial}{\partial t} \sum_{m=g,l,s} \left[\rho_m \alpha_m \left(u_m + \frac{1}{2} v_m^2 \right) \right] = \frac{\partial}{\partial z} \sum_{m=g,l,s} \left(\rho_m \alpha_m v_m \left(u_m + \frac{p}{\rho_m} + \frac{1}{2} v_m^2 \right) \right) + \sum_{m=g,l,s} (\rho_m \alpha_m v_m g \sin \theta) + \frac{Q_{\text{total}}}{A} + \sum_{m=g,l,s} \dot{H}_m - \alpha_s \phi T_h \frac{\rho_h}{M_h} \Delta H_h \quad (10)$$

2.4. Hydrate decomposition model

In the hydrate particle transport process, the solid–liquid two phase composed of hydrate particle and seawater flows upward along the wellbore. During upward flow, the hydrate will decompose with the rise of temperature and the reduce of pressure in the wellbore, and the complex gas–liquid–solid multiphase flow will emerge in the wellbore. Furthermore, the velocity of the hydrate particle in the wellbore have important effects in the decomposition rate. In order to calculate the hydrate dissociation rate in the wellbore, a dynamic decomposition model of hydrate under multiphase flow was established based on the Kim model (Kim et al., 1987). The hydrate dissociation rate expression is described as:

$$\dot{m}_h = \left(-\frac{dn_h}{dt} \right)_{T,p} = k_d A_h [f_{\text{eq}}(T, p_{\text{eq}}) - f(T, p)] \quad (11)$$

Since hydrate particle is a porous medium composed of hydrate and rock, the decomposition surface area of hydrate is related to the internal pore surface area of hydrate particle. Based on the fractal model, the specific surface area of the unit volume porous media can be expressed as (Zhou et al., 2018):

$$\sum S = \frac{6n}{m^6} \cdot \left[1 + m^{D_R-6} + \dots + (m^{D_R-6})^{i-1} \right] \quad (12)$$

$$k_d = \frac{1}{1/k_c + 1/k_f} = \frac{1}{1/k_c^0 e^{(-E_{\text{act}}/RT)} + 1/0.347(d_s v_m \rho_m / \mu_m)^{0.62} [\mu_m / (\rho_m D_{AB})]^{1/3} D_{AB} / d_s} \quad (19)$$

For Menger sponges, the model parameters are set as $m = 3$, $n = 7$, $D_R = 2.727$. Here, the hydrate particles are regarded as spherical, the effective dissociation area of hydrate particle is expressed as follows:

$$A_h = S_h \frac{\pi d_s^3}{6} \cdot \sum S \quad (13)$$

According to the definition of fugacity of pure matter, fugacity can be expressed as (Chen and Guo, 1998)

$$\begin{cases} dG = RT d \ln f \\ \lim_{p \rightarrow 0} \frac{f}{p} = 1 \end{cases} \quad (14)$$

In order to calculate the fugacity of gas, the fugacity coefficient is introduced here, which can be understood as the correction coefficient of pressure, and is expressed as follows:

$$\ln \left(\frac{f}{p} \right) = \frac{1}{RT} \int_{p^0}^p \left(V - \frac{RT}{p} \right) dp \quad (15)$$

Then, according to the Redlich-Kwong (R-K) equation of state of the methane gas, the pressure can be written as

$$p = \frac{RT}{V-b} - \frac{a}{T^{0.5} V(V+b)} \quad (16)$$

The coefficients of R-K equation are as follows

$$\begin{cases} a = \frac{0.72748 \cdot R^2 \cdot T_c^{2.5}}{p_c} \\ b = \frac{0.08664 \cdot R \cdot T_c}{p_c} \end{cases} \quad (17)$$

Then, the R-K equation is substituted into Eq. (15), the fugacity coefficient is derived as

$$\ln \left(\frac{f}{p} \right) = Z - 1 - \ln \left(Z - \frac{pb}{RT} \right) - \frac{a}{bRT^{1.5}} \ln \left(1 + \frac{b}{V} \right) \quad (18)$$

According to Ryokichi and Ripmeester's research, the decomposition rate constant of hydrate is expressed as (Wei et al., 2016)

2.5. Heat absorbed by hydrate decomposition

The heat absorbed by hydrate decomposition depends on the enthalpy change caused by the decomposition of hydrate into gas and liquid. The decomposition heat of hydrate can be obtained by the Clausius-Clapeyron equation (Clarke and Bishnoi, 2001; Sun et al., 2022):

$$\frac{d \ln p}{d(1/T)} = -\frac{\Delta H_h}{ZR} \quad (20)$$

Based on the comparative form of the Redlich-Kwong equation, the compression factor of methane gas is derived as

$$\frac{1}{Z \left(1 - 0.08664 \frac{p_r}{Z_r T_r} \right)} - \frac{0.42747 p_r}{Z^2 T_r^{2.47} \left(1 + 0.08664 \frac{p_r}{Z_r T_r} \right)} = 1 \quad (21)$$

According to the NGH phase equilibrium experiment, Chuai et al. (2019) obtained a lot of the NGH phase equilibrium data under wide ranges of temperature, pressure and NaCl concentration,

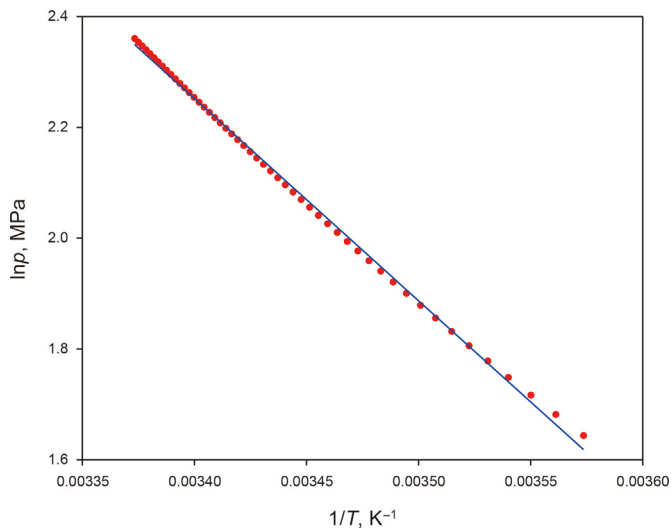


Fig. 3. The relationship curve between logarithm of equilibrium pressure and reciprocal of equilibrium temperature.

and obtained the NGH phase equilibrium equation with high accuracy and simple expression, which can be expressed as follows:

$$T_{eq}(\omega, p) = 247.2680 + 3.7167 \ln(26 - \omega) + 0.0793[\ln(26 - \omega)]^3 + \ln p \{ 9.5727 - 0.5479 \ln(26 - \omega) + 0.1049[\ln(26 - \omega)]^3 \} + (\ln p)^3 \{ -0.1189 + 0.0124 \ln(26 - \omega) - 0.0026[\ln(26 - \omega)]^3 \} + (\ln p)^5 \{ 0.0038 - 0.8144 \times 10^{-4} \ln(26 - \omega) + 0.3072 \times 10^{-4}[\ln(26 - \omega)]^3 \} \tag{22}$$

Fig. 3 shows the fitting linear relationship curve between logarithm of equilibrium pressure and reciprocal of equilibrium temperature under the condition of pure water. The relationship curve shows a roughly consistent linear relationship under any phase equilibrium condition. As can be seen from Fig. 3, the slope of the curve is -7763.7.

The calculated results of the dissociation heat were compared with those of Rueff et al. (1985), Huang et al. (2004) and Chen et al. (2019), as shown in Table 1. We can find that the results are in good follow the Rueff's experimental measure value with an error less than 0.3%.

3. Numerical solutions

The gas–liquid–solid multiphase flow model built in this paper is relatively complex, and the analytical solution of the model cannot be obtained directly, so it needs to adopt numerical method. Therefore, the four-point finite difference method is used to discretize the governing equation, and the iterative process is adopted to solve the discrete equations.

Table 1 Comparisons of calculation results of dissociation heat at 285 K.

Method	R–K equation	Setzmann equation	Calorimetry	P–R equation
Dissociation heat, kJ/mol	54.350	54.265	54.480	54.670
References	This paper	Chen et al. (2019)	Rueff et al. (1985)	Huang et al. (2004)

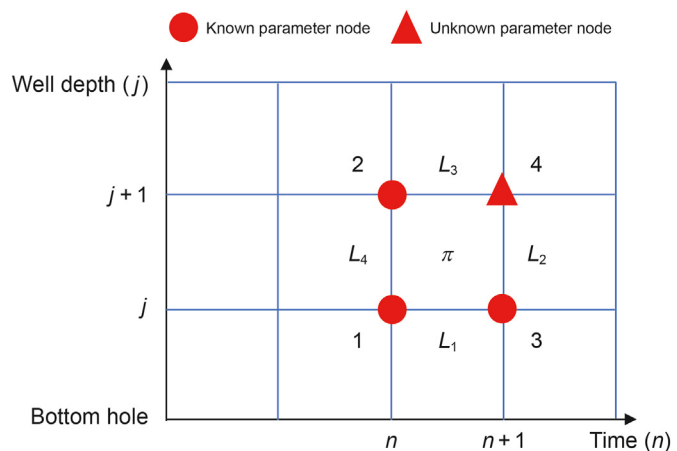


Fig. 4. Schematic diagram of grid difference in four-point difference scheme.

3.1. Meshing

A fixed-step method is used to divide the grid in the space. The length of the spatial grid section is as follows:

$$\Delta z_j = z_j - z_{j+1} = \Delta z \tag{23}$$

The time grid step is determined according to the mixing speed of multiphase flow and the length of spatial grid, as shown below:

$$\Delta t_n = \frac{\Delta z}{(v_m)_n} \tag{24}$$

3.2. Governing equation discretization

When the difference equations are established, the integral interpolation method is used to construct and the four-point difference scheme is selected. The specific form is described in Fig. 4.

The governing equations of model can be uniformly written into the following conservation form:

$$\frac{\partial X}{\partial t} + \frac{\partial Y}{\partial z} = Q \tag{25}$$

The integral form of Eq. (25) is as follows

$$\iint_{\pi} \left(\frac{\partial X}{\partial t} + \frac{\partial Y}{\partial z} \right) dzdt = 0 \tag{26}$$

The Eq. (26) is transformed into a curvilinear integral along the boundary of a region

$$\begin{aligned} \iint_{\pi} \left(\frac{\partial X}{\partial t} + \frac{\partial Y}{\partial z} \right) dzdt &= \oint_{\pi} Xdz - Ydt \\ &= - \int_{t_n}^{t_{n+1}} Y(t, z_j) dt + \int_{z_j}^{z_{j+1}} X(t_{n+1}, z) dz \\ &\quad + \int_{t_n}^{t_{n+1}} Y(t, z_{j+1}) dt - \int_{z_j}^{z_{j+1}} X(t_n, z) dz \\ &= 0 \end{aligned} \tag{27}$$

When Δt and Δz is small enough, the following difference format can be obtained:

$$\begin{aligned} (1 - F_w)(Y_{j+1}^n - Y_j^n) + F_w(Y_{j+1}^{n+1} - Y_j^{n+1}) \\ = \frac{\Delta z}{2\Delta t} (X_j^n + X_{j+1}^n - X_j^{n+1} - X_{j+1}^{n+1}) \end{aligned} \tag{28}$$

According to the above derivation, the difference equations corresponding to the governing equations of model can be obtained as follows:

The difference scheme of mass conservation equation of the gas phase:

$$\begin{aligned} (A\rho_g\alpha_g v_g)_{j+1}^{n+1} - (A\rho_g\alpha_g v_g)_j^{n+1} &= \frac{\Delta z}{2t} \left[(A\rho_g\alpha_g)_j^n - (A\rho_g\alpha_g)_{j+1}^n \right. \\ &\quad \left. - (A\rho_g\alpha_g)_j^{n+1} - (A\rho_g\alpha_g)_{j+1}^{n+1} \right] \\ &\quad + \frac{\Delta z}{2} \left[(A\alpha_s \dot{m}_g)_j^{n+1} \right. \\ &\quad \left. + (A\alpha_s \dot{m}_g)_{j+1}^{n+1} \right] \end{aligned} \tag{29}$$

The difference scheme of mass conservation equation of the liquid phase:

$$\begin{aligned} (A\rho_l\alpha_l v_l)_{j+1}^{n+1} - (A\rho_l\alpha_l v_l)_j^{n+1} &= \frac{\Delta z}{2t} \left[(A\rho_l\alpha_l)_j^n - (A\rho_l\alpha_l)_{j+1}^n \right. \\ &\quad \left. - (A\rho_l\alpha_l)_j^{n+1} - (A\rho_l\alpha_l)_{j+1}^{n+1} \right] \\ &\quad + \frac{\Delta z}{2} \left[(q_l - A\alpha_s \dot{m}_l)_j^{n+1} \right. \\ &\quad \left. + (q_l - A\alpha_s \dot{m}_l)_{j+1}^{n+1} \right] \end{aligned} \tag{30}$$

The difference scheme of mass conservation equation of the solid phase:

$$\begin{aligned} (A\rho_s\alpha_s v_s)_{j+1}^{n+1} - (A\rho_s\alpha_s v_s)_j^{n+1} &= \frac{\Delta z}{2t} \left[(A\rho_s\alpha_s)_j^n - (A\rho_s\alpha_s)_{j+1}^n \right. \\ &\quad \left. - (A\rho_s\alpha_s)_j^{n+1} - (A\rho_s\alpha_s)_{j+1}^{n+1} \right] \\ &\quad + \frac{\Delta z}{2} \left[(q_s - A\alpha_s \dot{m}_h)_j^{n+1} \right. \\ &\quad \left. + (q_s - A\alpha_s \dot{m}_h)_{j+1}^{n+1} \right] \end{aligned} \tag{31}$$

The difference scheme of mixed momentum conservation equation:

$$\begin{aligned} (Ap)_{j+1}^{n+1} - (Ap)_j^{n+1} &= \frac{\Delta z}{2\Delta t} \left\{ \left[\sum_{m=g,l,s} (\rho_m \alpha_m v_m A) \right]_j^n + \left[\sum_{m=g,l,s} (\rho_m \alpha_m v_m A) \right]_{j+1}^n \right\} \\ &\quad + \left\{ \left[\sum_{m=g,l,s} (\rho_m \alpha_m v_m^2 A) \right]_j^n \right. \\ &\quad \left. - \left[\sum_{m=g,l,s} (\rho_m \alpha_m v_m A) \right]_j^{n+1} - \left[\sum_{m=g,l,s} (\rho_m \alpha_m v_m A) \right]_{j+1}^{n+1} \right\} \\ &\quad - \left\{ \left[\sum_{m=g,l,s} (\rho_m \alpha_m v_m^2 A) \right]_{j+1}^{n+1} \right\} - \frac{\Delta z}{2} \left\{ \left[\sum_{m=g,l,s} (\rho_m \alpha_m) A g \sin \theta \right]_j^{n+1} + \left[\sum_{m=g,l,s} (\rho_m \alpha_m) A g \sin \theta \right]_{j+1}^{n+1} \right\} \\ &\quad - \frac{\Delta z}{2} \left[\left(A \frac{dp_f}{dz} \right)_j^{n+1} + \left(A \frac{dp_f}{dz} \right)_{j+1}^{n+1} \right] \end{aligned} \tag{32}$$

The difference scheme of energy conservation equation:

$$\begin{aligned}
 & \left\{ \sum_{m=g,l,s} \left[\rho_m \alpha_m V_m \left(u_m + \frac{p}{\rho_m} + \frac{1}{2} V_m^2 \right) \right] \right\}_{j+1}^{n+1} - \left\{ \sum_{m=g,l,s} \left[\rho_m \alpha_m V_m \left(u_m + \frac{p}{\rho_m} + \frac{1}{2} V_m^2 \right) \right] \right\}_j^{n+1} \\
 &= \frac{\Delta z}{2\Delta t} \left\{ \left[\sum_{m=g,l,s} \left(\rho_m \alpha_m \left(u_m + \frac{1}{2} V_m^2 \right) \right) \right]_j^n + \left[\sum_{m=g,l,s} \left(\rho_m \alpha_m \left(u_m + \frac{1}{2} V_m^2 \right) \right) \right]_{j+1}^n \right\} - \frac{\Delta z}{2} \left\{ \left[\sum_{m=g,l,s} (\rho_m \alpha_m) A g \sin \theta \right]_j^{n+1} \right. \\
 & \quad \left. + \left[\sum_{m=g,l,s} (\rho_m \alpha_m) A g \sin \theta \right]_{j+1}^{n+1} \right\} - \frac{\Delta z}{2} \left\{ \left[\frac{Q_{total}}{A} + \sum_{m=g,l,s} \dot{H}_m - \alpha_s \phi \Gamma_h \frac{\rho_h}{M_h} \Delta H_h \right]_j^{n+1} + \left[\frac{Q_{total}}{A} + \sum_{m=g,l,s} \dot{H}_m - \alpha_s \phi \Gamma_h \frac{\rho_h}{M_h} \Delta H_h \right]_{j+1}^{n+1} \right\} \quad (33)
 \end{aligned}$$

3.3. Solution procedure

In this paper, a double-cycle iterative calculation method is adopted, which first converges to pressure and then to temperature. The specific calculation steps are as follows Fig. 5.

4. Model validation

Although Japan and China have carried out experiments on decompression mining of hydrates in the ocean, the current research on hydrate solids fluidized mining is still in its infancy. In addition, the existing research on the multiphase flow law considering the phase transition of hydrates mainly focuses on the theoretical stage and lacks field test data. Therefore, it isn't easy to

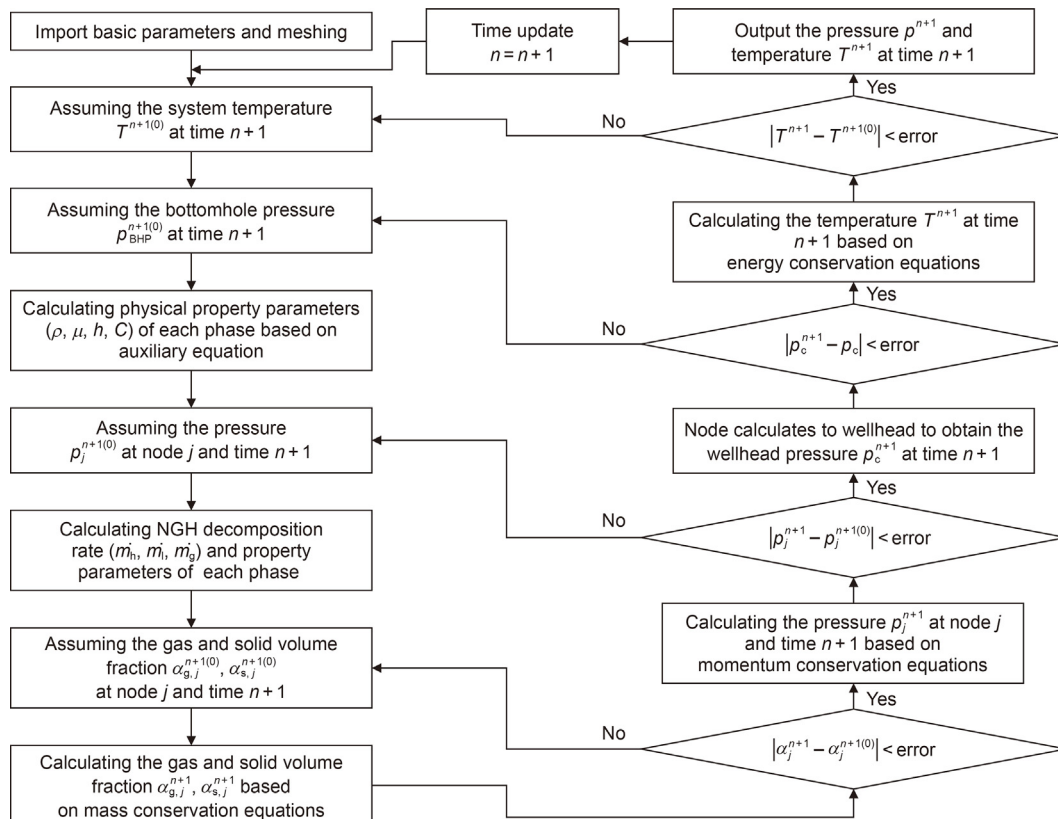


Fig. 5. Schematic of solution procedure.

Table 2
Basic parameters of the case well.

Parameter	Value
Depth of seawater, m	300
Depth of formation, m	4160
Pipeline outer diameter, m	0.152
Pipeline inner diameter, m	0.127
Injection rate, m ³ /s	0.024
Injection temperature, K	293.15
Porosity	–
Hydrate saturation	–
Water saturation	–
Temperature of sea surface, K	288.15
Geothermal gradient, K/m	0.025
Rate of penetration, m/h	10
Particles diameter, m	0.003
Wellhead backpressure, MPa	0.5

directly verify the accuracy of the model.

The model becomes a conventional wellbore multiphase flow model when ignoring the heat and mass transfer behavior caused by the hydrate phase change in the above model. At the same time, the physical meaning of heat and mass transfer caused by hydrate phase change in the model is apparent. Therefore, it is reasonable to use conventional measured wellbore temperature data to indirectly verify the above model because there is no field measured data. This paper used the measurement data of the MWD tool of a high-temperature and high-pressure well in the South China Sea for verification. Table 2 and Fig. 6 respectively present the basic parameters of case well and structure of the well.

Fig. 7(a) shows the variation of the calculated temperature and the measured temperature along the depth of the well during the process of drilling the bit from 3400 to 4000 m. It's easy to find from Fig. 7(a) that the calculated temperature and measured

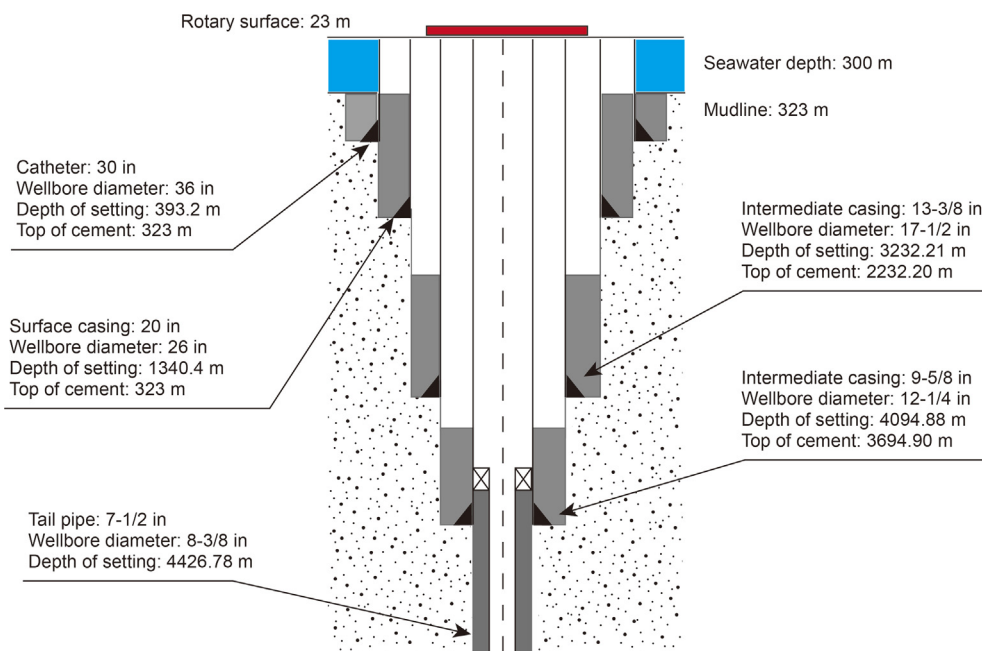


Fig. 6. Wellbore structure of case well.

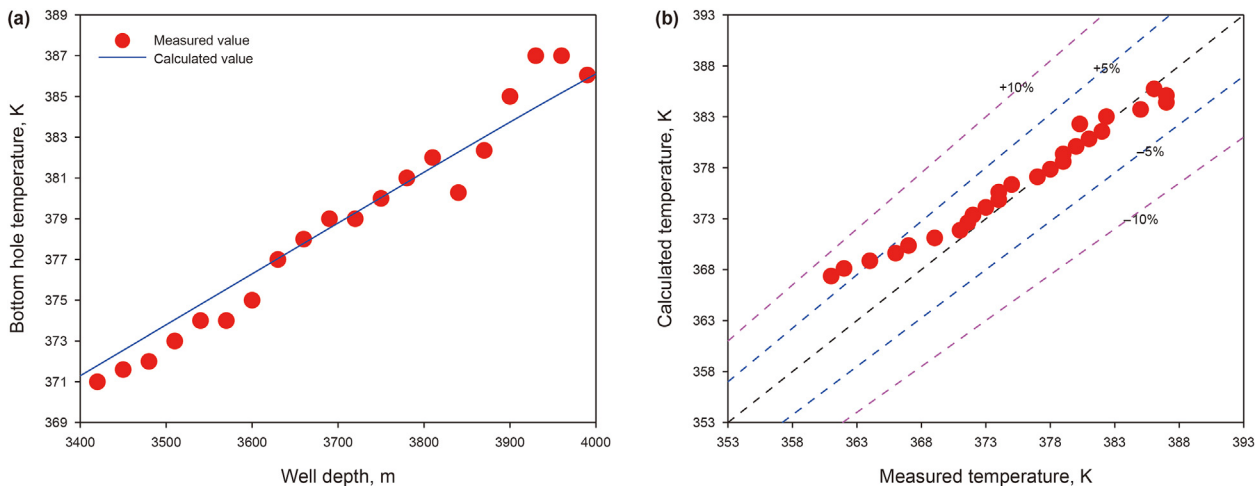


Fig. 7. Verification of field measured data. (a) Variation of calculated and the measured temperatures along well depth; (b) Error analysis of calculated temperature relative to measured temperature.

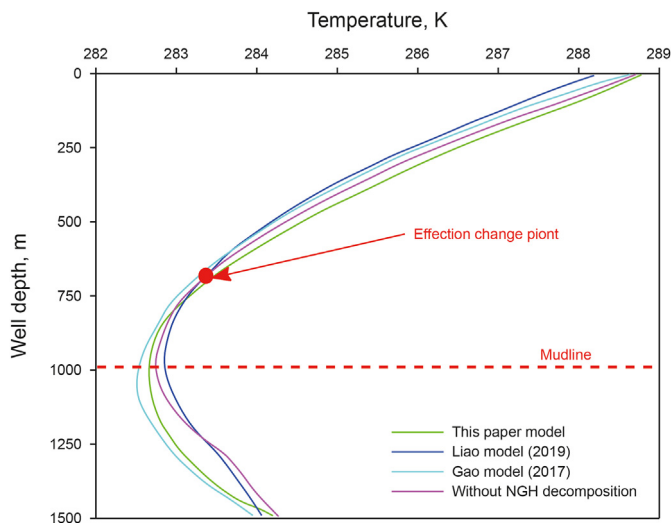


Fig. 8. Comparison of wellbore temperature distribution by adopting different models.

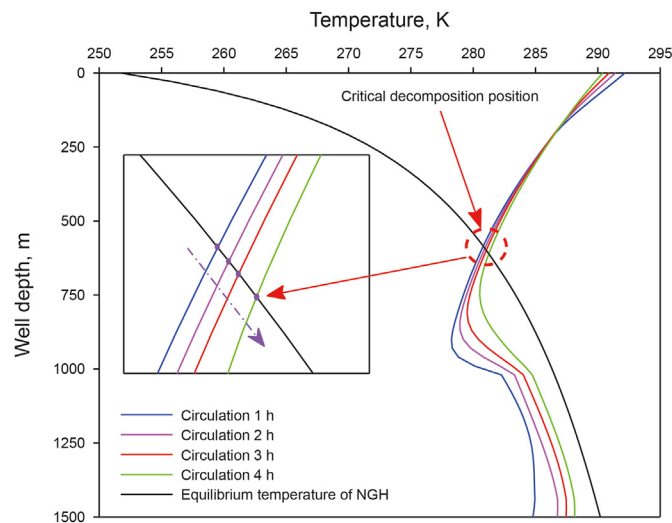


Fig. 9. Temperature profile of wellbore at different circulation time, and equilibrium temperature of hydrate.

Table 3
Basic parameters of simulation well.

Parameter	Value
Depth of seawater, m	1000
Depth of formation, m	1500
Pipeline outer diameter, m	0.508
Pipeline inner diameter, m	0.476
Injection rate, m ³ /s	0.030
Injection temperature, K	298.15
Porosity	0.45
Hydrate saturation	0.63
Water saturation	0.37
Temperature of sea surface, K	288.15
Geothermal gradient, K/m	0.024
Mining rate, kg/s	40
Particles diameter, m	0.003
Wellhead backpressure, MPa	0.5

temperature of the model have the same increasing trend with the depth of the well, and the agreement between the two is good. Fig. 7(b) shows a simple error analysis of the calculated temperature relative to the measured temperature. It can be seen from Fig. 7(b) that most of the errors in calculating the temperature do not exceed 5%, and the average error is 2.2%.

Fig. 8 compares the wellbore temperature by respectively adopted this paper model, the Gao model (Gao et al., 2017a, b), the Liao model (Liao et al., 2019), and the model that ignored the hydrate decomposition. It's easy to find from the figure that the variation trend of wellbore temperature calculated by each model is consistent, and the difference is basically within 5%. Besides, compared to without hydrate decomposition, it is essential to note that below affection change point, the wellbore temperature of hydrate production is lower than that of conventional oil and gas production. The main reason for the decrease of wellbore

temperature is the heat absorption caused by hydrate decomposition. However, above affection change point, the gas generated from hydrate decomposition reduce the thermal conductivity of the mixture fluid, resulting in higher wellbore temperature. This further proves the accuracy of the model.

5. Results and discussion

In order to study the influence of hydrate decomposition on multiphase flow characteristics of the wellbore during solid fluidized exploitation, a non-isothermal gas–liquid–solid transient flow model was established in this paper to carry out relevant numerical simulation research. Tables 3 and 4 show the relevant simulation parameters. Table 2 shows the basic simulation parameters, and Table 3 shows the thermodynamic parameters.

5.1. Results

The hydrate decomposition law and multiphase flow behavior in the wellbore under different cycle mining times are studied through the numerical simulation of the hydrate solid-state fluidized mining process.

5.1.1. Hydrate decomposition rate and region

Fig. 9 describes the hydrate decomposition regions under different circulation mining times. As shown from the figure, with the increase of mining time, the critical decomposition point of hydrate gradually moves down, and the decomposition region of hydrate in the wellbore gradually expands. Fig. 10 shows that the hydrate starts decomposition in around 500 m, and with the wellbore depth gradually decreases, the temperature of the wellbore increases and the pressure of the wellbore decreases, resulting in a gradual rise in the rate of hydrate decomposition.

Table 4
Thermodynamic parameters of medium.

Medium	Density, kg/m ³	Specific heat capacity, J/(kg·K)	Heat conductivity, J/(s·m·K)
Seawater	1025	3890	0.70
Hydrate	900	3100	0.52
Formation	2600	1200	2.10
String	7800	800	43.00

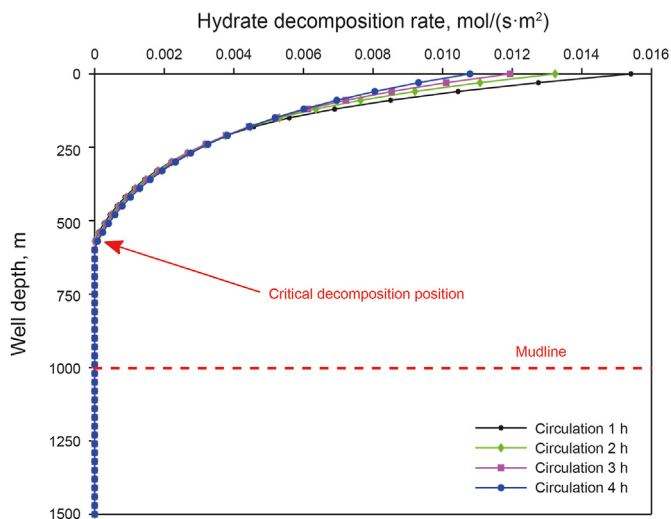


Fig. 10. Hydrate decomposition rate profile of wellbore at different circulation time.

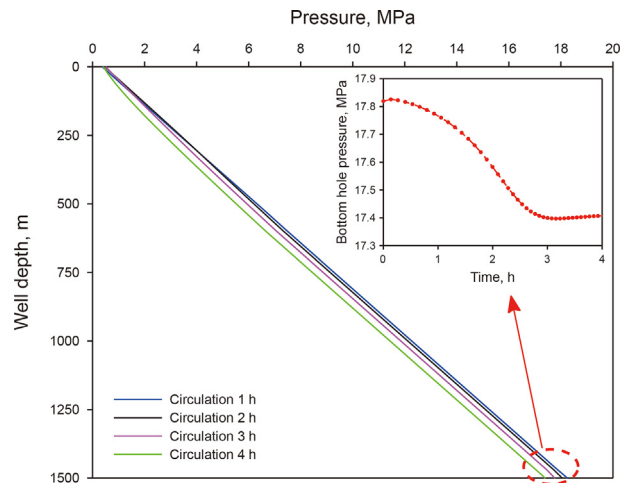


Fig. 13. Pressure distribution profile of wellbore at circulation time of 1, 2, 3, and 4 h.

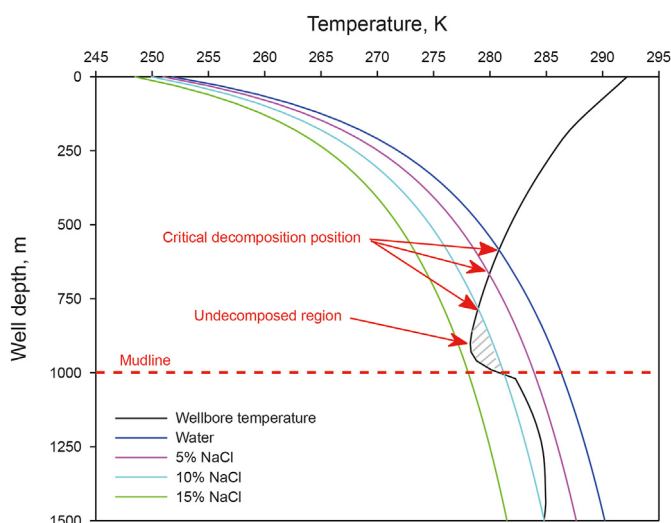


Fig. 11. Hydrate phase equilibrium temperature at NaCl concentration of 0, 5%, 10%, and 15%.

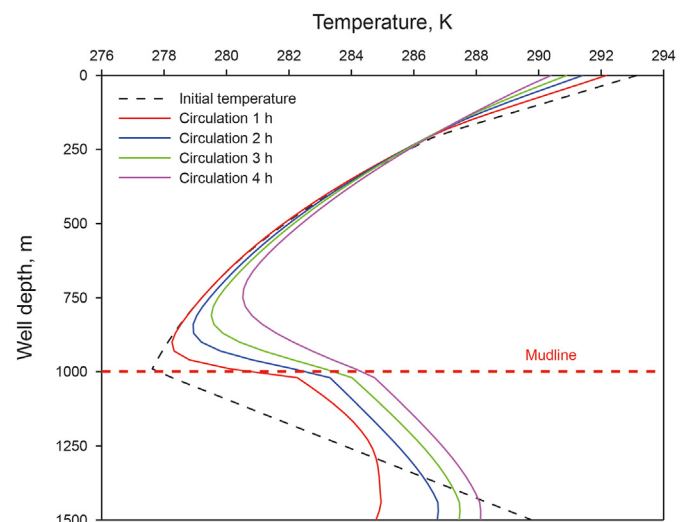


Fig. 14. Temperature distribution profile of wellbore at circulation time of 1, 2, 3, and 4 h.

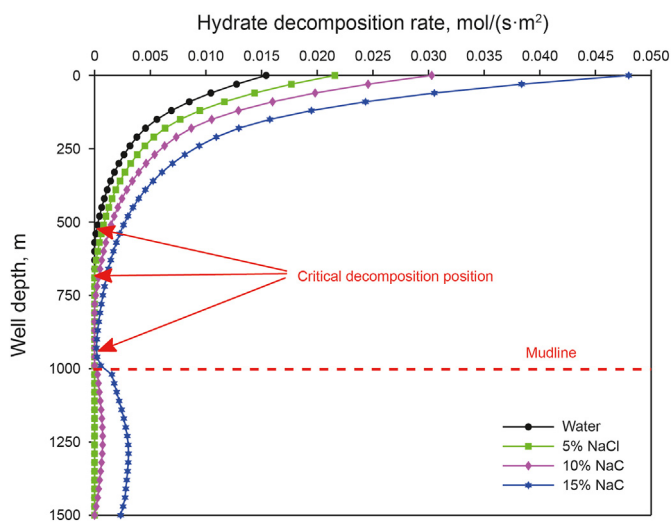


Fig. 12. Hydrate decomposition rate at NaCl concentration of 0, 5%, 10%, and 15%.

Besides, in the near wellhead, the decomposition rate of hydrate reduces with the increase of time. This is mainly because the hydrate decomposition is an endothermic reaction. With the rise of time, the heat absorbed by the decomposition reaction increases accordingly. Moreover, the wellbore heat cannot supplement timely, resulting in decreased wellbore temperature and the hydrate decomposition rate.

Fig. 11 shows the hydrate decomposition regions under different NaCl mass fractions. It can be found that with the rise of NaCl concentration in seawater, the methane hydrate phase's equilibrium temperature decreases, leading to the gradual expansion of hydrate decomposition areas in the wellbore. When the NaCl mass fraction reaches 10%, the hydrate will start decomposition at the bottom of the well. When the NaCl mass fraction reaches 15%, the hydrate decomposition area will be expanded to the whole wellbore. Fig. 12 shows that near the mudline, the decomposition rate of hydrate is the lowest. Above the critical decomposition point, the decomposition rate of hydrate rises with the reduce of well depth. Besides, NaCl mass fraction growth will result in a significant increase in the decomposition rate of hydrate. During the solid fluidization mining of hydrate, appropriately increasing NaCl

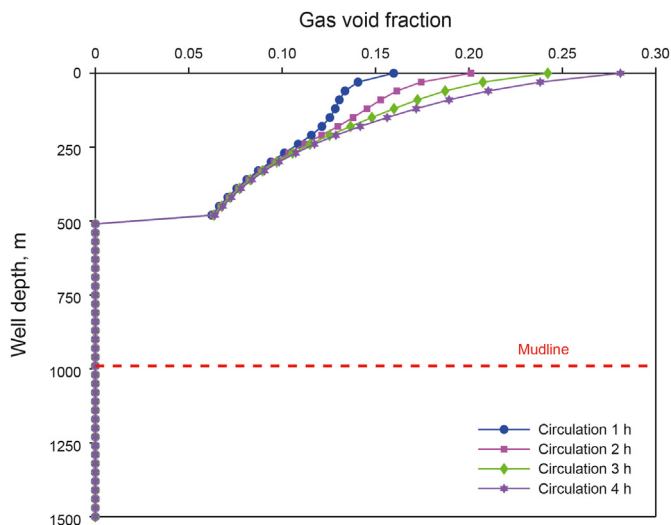


Fig. 15. Gas volume fraction distribution profile at circulation time of 1, 2, 3, and 4 h.

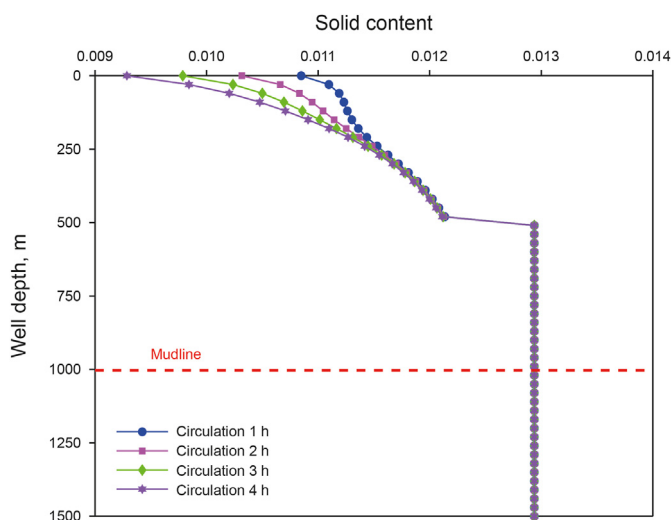


Fig. 16. Solid volume fraction distribution profile at circulation time of 1, 2, 3, and 4 h.

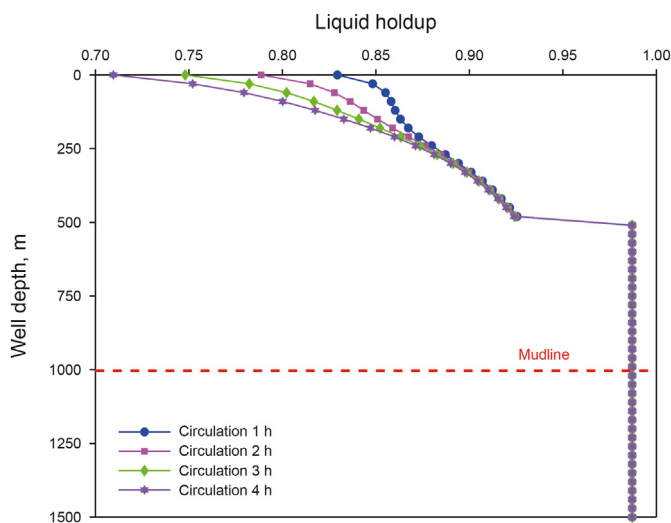


Fig. 17. Liquid volume fraction distribution profile at circulation time of 1, 2, 3, and 4 h.

concentration can expand the hydrate decomposition areas and increase the hydrate decomposition rate to improve gas production and reduce the difficulty of later treatment.

5.1.2. Pressure and temperature distribution profile

Figs. 13 and 14 respectively describe temperature and pressure profiles of wellbore at different mining times. It can be found from Fig. 13 that the pressure of the wellbore gradually decreases with the rise of time. It notes that the bottom hole pressure decreases by about 0.4 MPa when exploited for 4 h. The main reason for the decrease in wellbore pressure is that the gas produced by the decomposition of hydrate reduces the density of the mixed fluid and the pressure drop of gravity.

As can be seen from Fig. 14, with well depth decreases, the wellbore temperature firstly falls and then increases, and the wellbore temperature in the near mudline reaches the lowest. In addition, as time increases, in the lower wellbore section, heat continuously flows from the formation to the bottom of the well, and the temperature of the wellbore gradually increases. In the upper wellbore section, Increased heat exchange between wellbore fluid and surrounding media and the hydrate decomposes absorbs heat, which ultimately leads to a decrease in the wellbore temperature.

5.1.3. Gas-fluid-solid three-phase volume fraction distribution profile

Figs. 15–17, respectively, show the gas-fluid-solid three-phase volume fraction distribution profile at circulation time of 1, 2, 3, and 4 h. It can be found from Fig. 15 the hydrate began to decompose around 500 m. With the increased time, the amount of hydrate decomposition gradually increased, resulting in the gradual increase in volume fraction of gas in the wellbore. Simultaneously, it notes from Figs. 16 and 17 that the volume fraction of liquid and solid in the wellbore gradually decrease with increased time.

Besides, with the wellbore's depth decreases, the volume fraction of gas gradually increases. The main reason for the increase in gas volume fraction is the increase of decomposition rate of hydrate and the rise in gas expansion due to the decrease of wellbore pressure.

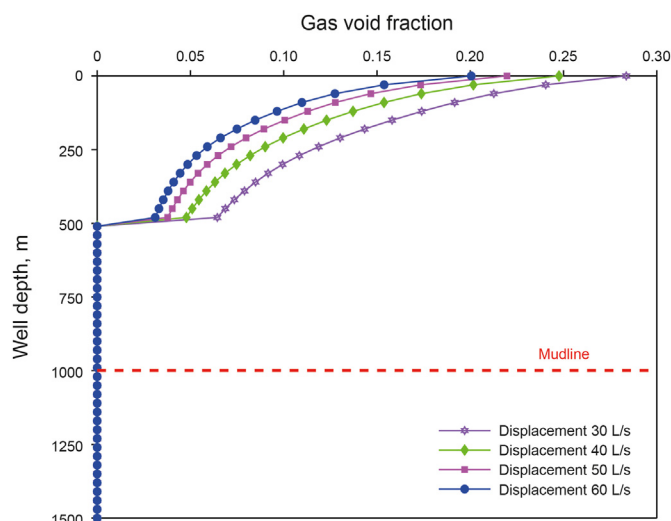


Fig. 18. Gas volume fraction distribution profile of wellbore under different flow rates.

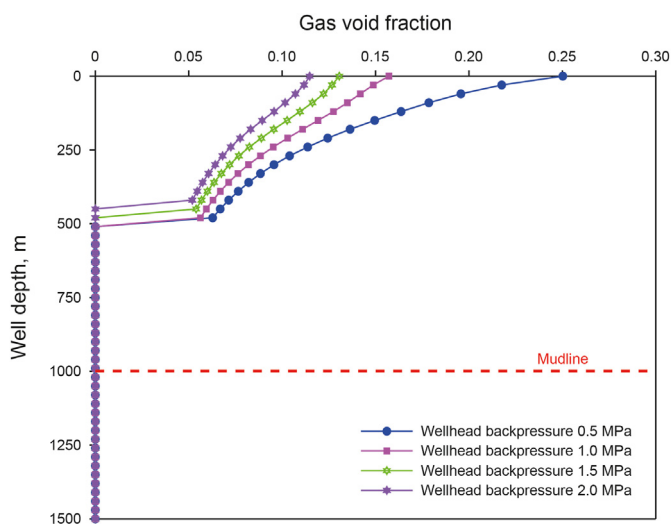


Fig. 19. Gas volume fraction distribution profile of wellbore under different wellhead backpressures.

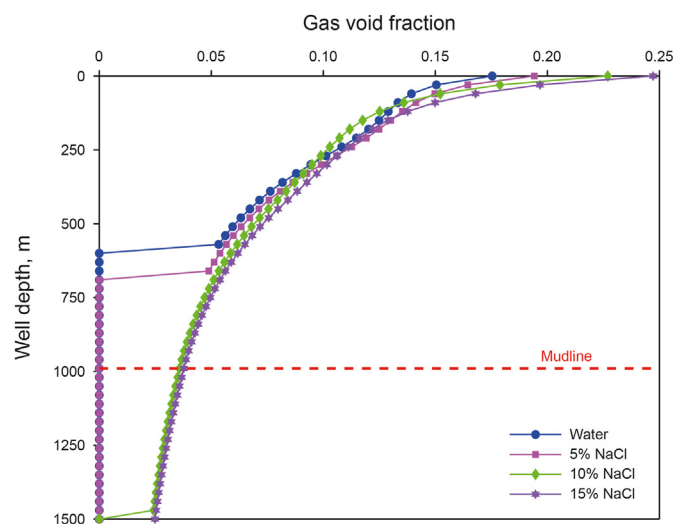


Fig. 21. Gas volume fraction distribution profile of wellbore under different NaCl concentrations.

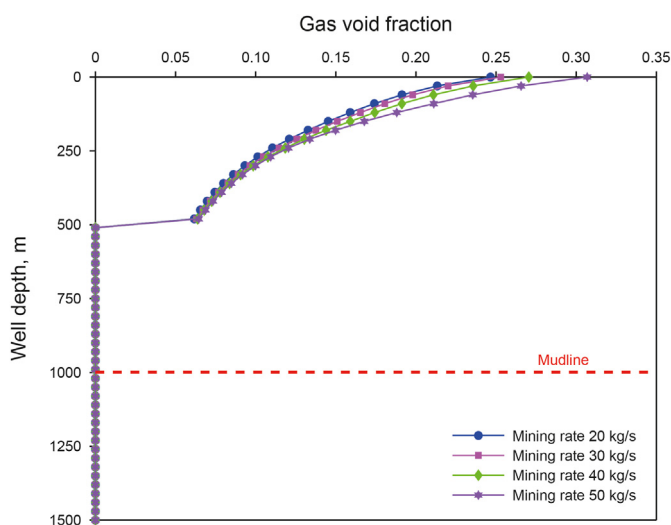


Fig. 20. Gas volume fraction distribution profile of wellbore under different mining rates.

5.2. Discussion

During the solid fluidization mining of hydrate, it's of great significance to know the distribution law of gas-phase volume fraction in wellbore under different mining parameters for safe and efficient mining of hydrate. Therefore, this paper researched the effect of critical parameters such as mining rate, flow rate, wellhead backpressure, and salt concentration on gas-phase volume fraction distribution in the wellbore.

Fig. 18 describes the distribution profile of gas volume fraction in the wellbore at different flow rates. It's easy to find that the volume fraction of gas increases gradually with the increase of flow rate. The increase in liquid flow rate will lead to the heat exchange between the hydrate particles and the surrounding fluid increases, which increases the decomposition rate of the hydrate and ultimately causes the volume fraction of the gas phase in the wellbore to continue to rise.

Fig. 19 depicts the distribution characteristics of the volume fraction of gas in the wellbore under different wellhead

backpressures. When improving the wellhead backpressure, the wellbore pressure profile will increase overall. The increase in wellbore pressure will reduce the driving force and decomposition rate of hydrate decomposition and ultimately lead to a decrease in gas volume fraction. In addition, the increase in wellhead backpressure will cause the critical point of hydrate decomposition to rise, which reduces the hydrate decomposition area in the wellbore. Therefore, in the process of hydrate mining, the volume fraction profile of each phase in the wellbore can be controlled by adjusting the wellhead backpressure to ensure safe and efficient transportation of hydrate.

Fig. 20 shows the distribution of gas volume fractions at different hydrate mining rates. It can be seen from the figure that with the increase in the hydrate mining rate, the hydrate content in the wellbore increases, thus increasing the hydrate decomposition rate in the wellbore, and ultimately leading to the increase in the volume fraction of gas in the wellbore. In addition, it is easy to find that the increase in gas phase volume fraction in the wellbore increases gradually with the increase in mining rate. Therefore, we should reasonably control the mining rate in the process of hydrate solid-state fluidization mining to ensure wellbore safety.

Fig. 21 depicts the distribution of gas volume fraction in the wellbore at different NaCl mass fractions. It is not difficult to find that the increase in NaCl concentration in seawater will expand the decomposition range of hydrate in the wellbore and increase the decomposition rate of hydrate. Therefore, reasonable control of the salt concentration of the injected seawater will help control the decomposition area of the hydrate in the wellbore and ensure the efficient transportation of hydrate particles.

6. Conclusions

Considered the coupling relationship between dynamic decomposition of hydrate, multiphase flow, and system heat transfer, this paper developed a non-isothermal transient multiphase flow mechanism model during the solid fluidization mining of hydrate. The hydrate decomposition rate, hydrate decomposition region, and multiphase flow law were studied through numerical simulation. Meanwhile, the effect of key mining parameters such as wellhead backpressure, liquid flow rate, mining rate, and salt concentration are analyzed. The main conclusions of this research are as follows:

- (1) During the solid fluidization exploitation of hydrate, with the rise of time, the decomposition area of hydrate in the wellbore gradually expands, and the hydrate decomposition rate gradually decreases. Increasing NaCl concentration in seawater helps widen hydrate decomposition area in the wellbore and improves hydrate decomposition rate. When the NaCl mass fraction in seawater reaches 15%, the hydrate decomposition regions will expand to the whole wellbore.
- (2) As the production time increases, the wellbore pressure gradually decreases. When the mining time is 4 h, the bottom hole pressure drops by about 0.4 MPa. At the same time, during the mining process, the wellbore temperature at the lower part of the well gradually rises. In contrast, the wellbore temperature in the upper section of the well decreases slowly, and the wellbore temperature near the mudline is the lowest.
- (3) After the particles of hydrate arrive at the wellhead, the volume fraction of each phase in the wellbore gradually tends to be stable with the increase in mining time. After 4 h of mining, the gas volume fraction can reach about 30%, which will lead to lower wellbore carrying efficiency.
- (4) Increasing fluid flow rate is beneficial to improve hydrate decomposition rate. Increasing wellhead backpressure will reduce the hydrate decomposition area. When wellhead backpressure rises to 2 MPa, the wellbore volume fraction will reduce to about 12%. The increase in mining rate will lead to the volume fraction of gas in the wellbore.

Declaration of competing interest

The authors declare that they have no known competing financial interests or personal relationships that could have appeared to influence the work reported in this paper.

Acknowledgements

This research work was supported by the Youth Program of National Natural Science Foundation of China (Grant No. 52104012), the Key Program of the National Natural Science Foundation of China (Grant No. 51734010), and the Key Natural Science Projects of Scientific Research Plan in Colleges and Universities of Xinjiang Uygur Autonomous Region (Grant No. XJEDU20211028).

References

Bai, Y., Li, Q., Li, X., Du, Y., 2009. Numerical simulation on gas production from a hydrate reservoir underlain by a free gas zone. *Chin. Sci. Bull.* 54 (5), 865–872. <https://doi.org/10.1007/s11434-008-0575-z> (in Chinese).

Boswell, R., Collett, T.S., 2011. Current perspectives on gas hydrate resources. *Energy Environ. Sci.* 4 (4), 1206–1215. <https://doi.org/10.1039/c0ee00203h>.

Chen, G.J., Guo, T.M., 1998. A new approach to gas hydrate modelling. *Chem. Eng. J.* 71 (2), 145–151. [https://doi.org/10.1016/S1385-8947\(98\)00126-0](https://doi.org/10.1016/S1385-8947(98)00126-0).

Chen, H., Guan, F.J., Xiao, Q., et al., 2019. A new method for calculating the dissociation heat of methane hydrate. *Contemp. Chem. Ind.* 48 (8), 1783–1786. <https://doi.org/10.13840/j.cnki.cn21-1457/tq.2019.08.038> (in Chinese).

Chuai, S.Y., Wang, H.N., Zhang, N., et al., 2019. 3-D Phase equilibrium surface equation of methane hydrate considering the effect of temperature, pressure and salt concentration. *Oil and Gas Chemicals* 48, 49–55. <https://doi.org/10.3969/j.issn.1007-3426.2019.05.010> (in Chinese).

Clarke, M., Bishnoi, P.R., 2001. Determination of the activation energy and intrinsic rate constant of methane gas hydrate decomposition. *Can. J. Chem. Eng.* 79 (1), 143–147. <https://doi.org/10.1002/cjce.5450790122>.

Gao, Y., Cui, Y., Xu, B., et al., 2017a. Two phase flow heat transfer analysis at different flow patterns in the wellbore. *Appl. Therm. Eng.* 117, 544–552. <https://doi.org/10.1016/j.applthermaleng.2017.02.058>.

Gao, Y., Sun, B., Xu, B., et al., 2017b. A wellbore/formation-coupled heat-transfer model in deepwater drilling and its application in the prediction of hydrate-reservoir dissociation. *SPE J.* 22 (3), 756–766. <https://doi.org/10.2118/184398-PA>.

Ghobadpouri, S., Hajidavalloo, E., Noghrehabadi, A.R., 2017. Modeling and simulation of gas–liquid–solid three-phase flow in under-balanced drilling operation. *J. Petrol. Sci. Eng.* 156, 348–355. <https://doi.org/10.1016/j.petrol.2017.06.015>.

Guo, Y., Sun, B., Zhao, K., et al., 2016. A prediction method of natural gas hydrate formation in deepwater gas well and its application. *Petroleum* 2 (3), 296–300. <https://doi.org/10.1016/j.petim.2016.06.004>.

He, M., 2016. *Research on Real-Time Interpretation Theory and Control Method of Managed-Pressure Drilling Overflow*. Doctoral Dissertation. China University of Petroleum at Beijing.

Huang, W.J., Liu, D.P., Zhou, W.Z., et al., 2004. Thermophysical properties of natural gas hydrate. *Nat. Gas. Chem. Ind.* 29, 66–71. <https://doi.org/10.3969/j.issn.1001-9219.2004.04.016> (in Chinese).

Kim, H.C., Bishnoi, P.R., Heidemann, P.A., Rizvi, S.S.H., 1987. Kinetics of methane hydrate decomposition. *Chem. Eng. Sci.* 42, 1645–1653. [https://doi.org/10.1016/0009-2509\(87\)80169-0](https://doi.org/10.1016/0009-2509(87)80169-0).

Li, P., Zhang, X., Lu, X., et al., 2019. Three-dimensional Eulerian modeling of gas–liquid–solid flow with gas hydrate dissociation in a vertical pipe. *Chem. Eng. Sci.* 196, 145–165. <https://doi.org/10.1016/j.ces.2018.10.053>.

Liao, Y., Sun, X., Sun, B., et al., 2019. Transient gas–liquid–solid flow model with heat and mass transfer for hydrate reservoir drilling. *Int. J. Heat Mass Tran.* 141, 476–486. <https://doi.org/10.1016/j.ijheatmasstransfer.2019.06.097>.

Merey, S., 2016. Drilling of gas hydrate reservoirs. *J. Nat. Gas Sci. Eng.* 35, 1167–1179. <https://doi.org/10.1016/j.jngse.2016.09.058>.

Rueff, R.M., Sloan, E.D., Yesavage, V.F., 1985. Heat capacity and heat of dissociation of methane hydrates: a new approach. *AIChE J.* 34 (9), 1468–1476. <https://doi.org/10.1002/aic.690340908>.

Shi, H., Holmes, J.A., Durlinsky, L.J., et al., 2005. Drift-flux modeling of two-phase flow in wellbores. *SPE J.* 10 (1), 24–33. <https://doi.org/10.2118/84228-PA>.

Shishavan, R.A., Hubbell, C., Perez, H., et al., 2015. Combined rate of penetration and pressure regulation for drilling optimization by use of high-speed telemetry. *SPE Drill. Complet.* 30 (1), 17–26. <https://doi.org/10.2118/170275-PA>.

Sun, B., Wang, Z.G., Gong, P., et al., 2011. Application of a seven-component multiphase flow model to deepwater well control. *Acta Pet. Sin.* 32 (6), 1042. <https://doi.org/10.7623/syxb201106018> (in Chinese).

Sun, S.C., Gu, L., Yang, Z.D., et al., 2022. Thermophysical properties of natural gas hydrates: a reviews. *Nat. Gas. Ind.* 9 (3), 246–263. <https://doi.org/10.1016/j.ngib.2022.04.003> (in Chinese).

Sun, X., Sun, B., Wang, Z., et al., 2018. A hydrate shell growth model in bubble flow of water-dominated system considering intrinsic kinetics mass and heat transfer mechanisms. *Int. J. Heat Mass Tran.* 117, 940–950. <https://doi.org/10.1016/j.ijheatmasstransfer.2017.10.045>.

Sun, Y., Cai, F., Li, Q., et al., 2020. Evaluation of marine shallow surface natural gas hydrate resources. *Marine Geology Frontiers* 36 (9), 87–93. <https://doi.org/10.16028/j.1009-2722.2020.061> (in Chinese).

Wang, Z., Sun, B., 2009. Annular multiphase flow behavior during deep water drilling and the effect of hydrate phase transition. *Petrol. Sci.* 6 (1), 57–63. <https://doi.org/10.1007/s12182-009-0010-3>.

Wang, Z., Zhao, Y., Sun, B., et al., 2016. Modeling of hydrate blockage in gas-dominated systems. *Energy Fuel.* 30 (6), 4653–4666. <https://doi.org/10.1021/acs.energyfuels.6b00521>.

Wei, N., Sun, W., Meng, Y., et al., 2016. Sensitivity analysis of multiphase flow in annulus during drilling of marine natural gas hydrate reservoirs. *J. Nat. Gas Sci. Eng.* 36, 692–707. <https://doi.org/10.1016/j.jngse.2016.11.007>.

Wei, N., Zhao, J., Sun, W., et al., 2019. Non-equilibrium multiphase wellbore flow characteristics in solid fluidization exploitation of marine gas hydrate reservoirs. *Nat. Gas. Ind.* 6 (3), 282–292. <https://doi.org/10.1016/j.ngib.2018.10.008> (in Chinese).

Yang, H., Li, J., Liu, G., et al., 2019a. A transient hydro-thermo-bubble model for gas kick simulation in deep water drilling based on oil-based mud. *Appl. Therm. Eng.* 158, 113776. <https://doi.org/10.1016/j.applthermaleng.2019.113776>.

Yang, P., Wang, G., Zhou, S., et al., 2019b. Development and application of simulation experimental device for solid fluidization of non-diagenetic gas hydrate. *Chin. J. Rock Mech. Eng.* 38 (S2), 3512–3519. <https://doi.org/10.13722/j.cnki.jrme.2019.0415> (in Chinese).

Zhao, J., Zheng, J.N., Wang, X., Dong, S., Yang, M., Song, Y., 2022. Effects of underlying gas on formation and gas production of methane hydrate in muddy low-permeability cores. *Fuel* 309, 122128. <https://doi.org/10.1016/j.fuel.2021.122128>.

Zhao, J., Zhou, S., Zhang, L., et al., 2017. The first global physical simulation experimental systems for the exploitation of marine natural gas hydrates through solid fluidization. *Nat. Gas. Ind.* 37 (9), 15–22. <https://doi.org/10.3787/j.issn.1000-0976.2017.09.002> (in Chinese).

Zhou, S., Chen, W., Li, Q., et al., 2017. Research on the solid fluidization well testing and production for shallow non-diagenetic natural gas hydrate in deep water area. *China Offshore Oil Gas* 29 (4), 1–8. <https://doi.org/10.11935/j.issn.1673-1506.2017.04.001> (in Chinese).

Zhou, S., Zhao, J., Li, Q., et al., 2018. Optimal design of the engineering parameters for the first global trial production of marine natural gas hydrates through solid fluidization. *Nat. Gas. Ind.* 5 (2), 118–131. <https://doi.org/10.3787/j.issn.1000-0976.2017.09.001> (in Chinese).

Zuber, N., Findlay, J.A., 1965. Average volumetric concentration in two phase flow systems. *J. Heat Tran.* 87 (4), 453–468. <https://doi.org/10.1115/1.3689137>.